Energy Advances

ROYAL SOCIETY OF CHEMISTRY

PAPER

View Article Online
View Journal | View Issue

Cite this: *Energy Adv.*, 2024, 3, 1047

Enhanced OH^- conductivity from 3D alkaline graphene oxide electrolytes for anion exchange membrane fuel cells†

Nonoka Goto,‡[a] Mohammad Atiqur Rahman,‡[abc] Md. Saidul Islam,[ae] Ryuta Tagawa,[a] Chiyu Nakano,[d] Muhammad Sohail Ahmed,[e] Yoshihiro Sekine,[af] Yuta Nishina,[d] Shintaro Ida[e] and Shinya Hayami *[aeg]

Received 30th January 2024,
Accepted 13th April 2024

DOI: 10.1039/d4ya00059e

rsc.li/energy-advances

A promising green energy technology, anion exchange membrane fuel cells (AEMFCs) offer several advantages over proton exchange membrane fuel cells (PEMFCs), including lower cost, higher durability, and improved effectiveness. However, the widespread commercialization of AEMFCs has been hindered by the lack of low-cost, high-conductivity anion-exchange membranes (AEMs). This work reports the fabrication of a high-conductivity OH^- ion exchange membrane using simple freeze-drying of graphene oxide at pH = 11 (3DGO11). At 25 °C and 100% RH conditions, the resulting membrane exhibits a through-plane hydroxide ion conductivity of 1.93×10^{-4} S cm^{-1} and an in-plane conductivity of 3.74×10^{-2} S cm^{-1}. This high conductivity is attributed to the high porosity and multi-directional ion transport pathways created by the three-dimensional alkaline graphene oxide structure. These findings suggest a route for the development of cost-effective and high-performance AEMFCs.

1. Introduction

Proton exchange membrane fuel cells (PEMFCs) have achieved a significant milestone by introducing the first commercially available fuel-cell automobile. Fuel cell vehicles, powered by PEMFCs, present a compelling alternative to battery electric vehicles, offering an extended range and faster refuelling. Commercially, perfluorosulfonic acid (PFSA) membranes, such as Nafion, have been widely considered as the standard proton exchange membrane (PEM) for PEMFCs, due to their elevated chemical stability under a strong radical environment, high mechanical stability and high proton conductivity. Unfortunately, complex synthetic route, high cost and high fuel crossover restrict their use.[1a] Additionally, the widespread adoption of PEMFC technology faces a challenge due to the necessity for expensive platinum group metals (PGMs) and their alloys as electrocatalysts in the highly acidic environment of PEMFCs, limiting their commercial viability.[1b] Addressing this limitation, anion exchange membrane fuel cells (AEMFCs) and electrolysers have emerged as promising technologies for generating green power and fuels. These technologies offer several advantages, including using non-platinum group metals (non-PGM) as catalysts, low fuel crossover, durability, and excellent dynamic reactivity. The applications of anion exchange membranes (AEMs) are diverse, encompassing fields such as hydrometallurgy, heavy metal recovery, water treatment, and the electrochemical industry. AEMs play a crucial role in hydrogen production through water electrolysis, metal electrodeposition, electrodialysis technology, energy storage, and cell technology.[2–4] In AEMFCs, the solid electrolyte membrane is a physical barrier between electrodes and feed gases, facilitating effective OH^- ion transport and providing essential mechanical support to the cell's catalyst layers. The development of robust and high-performing AEMs has garnered considerable attention, driven by the ongoing advancements in AEMFCs and anion exchange membrane electrolyser cells (AEMECs) as potentially more economical and sustainable alternatives to

[a] *Department of Chemistry, Graduate School of Science and Technology, Kumamoto University, 2-39-1 Kurokami, Chuo-ku, Kumamoto 860-8555, Japan. E-mail: hayami@kumamoto-u.ac.jp*
[b] *Department of Chemistry, Comilla University, Cumilla-3500, Bangladesh*
[c] *International Research Organization for Advanced Science and Technology, Kumamoto University, 2-39-1 Kurokami, Chuo-ku, Kumamoto 860-8555, Japan*
[d] *Research Core for Interdisciplinary Sciences, Okayama University Professor (Research), Graduate School of Natural Science and Technology, Okayama University, Okayama, Japan*
[e] *Institute of Industrial Nanomaterials (IINa), Kumamoto University, 2-39-1 Kurokami, Chuo-ku, Kumamoto 860-8555, Japan*
[f] *Priority Organization for Innovation and Excellence, Kumamoto University, 2-39-1 Kurokami, Chuo-ku, Kumamoto 860-8555, Japan*
[g] *International Research Center for Agricultural and Environmental Biology (IRCAEB), 2-39-1 Kurokami, Chuo-ku, Kumamoto 860-8555, Japan*

† Electronic supplementary information (ESI) available. See DOI: https://doi.org/10.1039/d4ya00059e

‡ These authors contributed equally.

their proton exchange membrane counterparts.[5,6] Many commercial anion exchange membranes are composed of a fluorocarbon or hydrocarbon polymer backbone containing cationic functional groups that serve as anion conduction sites, including quaternary ammonium ($-NR_3^+$), phosphonium, sulfonium, or metal base functional groups. Various researchers have contributed to developing a wide range of anion exchange membranes.[7–9] J. Yoo *et al.* have synthesized quaternary amines from cross-linked compounds with Br^- counter ions in a PPO/PDAD membrane showing promise for AEMs based on their ionic physicochemical immobility and hydroxide conductivity.[9b] Additionally, functionalised graphene oxide nanofiber has been found to be an excellent nano filler for enhancing the performance of AEMs.[9c,d] However, creating high-performance and durable anion exchange membranes faces challenges, including polymer degradation under operational conditions, lower conductivity of OH^- ions compared to H^+, and partial dissociation of quaternary cations. Additionally, the complex and potentially toxic synthetic procedures involved in polymer fabrication add further difficulties to produce polymer-based membranes. Overcoming these challenges is crucial for advancing the practical application of anion exchange membrane technologies in the field of electrochemical energy conversion.[10,11]

Graphene oxide (GO) has garnered significant attention in the realm of electrochemical energy conversion devices due to its cost-effectiveness, straightforward synthetic methods, remarkable chemical and thermal stability, tuneable pore size, high surface area, robust oxygen-containing functional groups (including epoxy, hydroxyl, carboxylic acid, *etc.*), impressive mechanical strength, and atomic-level thickness.[12–15] The incorporation of oxygen functional groups on the edges and basal planes of GO not only facilitates water retention but also demonstrates efficient H^+ ion conduction, leading to enhanced proton exchange membrane fuel cell performance. Moreover, the broad intercalation chemistry and facile functionalization of GO contribute to improved conducting properties.[16–22] To fine-tune GO's chemical properties, the aqueous dispersion's pH can be controlled under ambient conditions, allowing for versatile applications. Under alkaline conditions, reversible epoxy–hydroxyl conversions occur in the epoxy groups of GO, accompanied by changes in the electronic states of the GO sheets.[23] Previous research from our group revealed the pH-dependent switch in ion conduction properties of GO between H^+ and OH^- while we observed that the vacuum filtration-driven GO membrane shows OH^- conductivity at pH = 11 (2DGO11).[22] However, conventional vacuum filtration methods often result in stacked GO layers, limiting ion movement and lowering conductivity, particularly with larger hydrated hydroxide ions. Addressing these challenges, Hayami *et al.* proposed a novel approach to boost ionic conductivity through the structural conversion of GO in the third direction, employing a freeze-drying method that maintains hydrophilic functional groups. The resulting three-dimensional graphene oxide (3DGO) exhibits heightened porosity, an enhanced interlayer space, and an interconnected network. Proton conductivity measurements in the through-plane direction demonstrated a 175-fold increase compared to GO membranes fabricated using the vacuum filtration method (Scheme 1).[24]

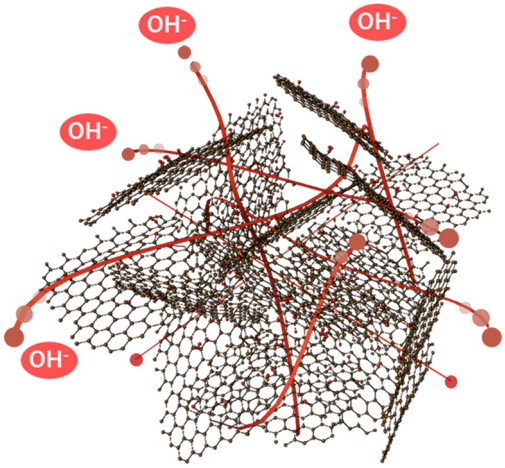

Scheme 1 OH^- ion conductivity using three-dimensional alkaline graphene oxide.

Motivated by these findings, our present work focuses on fabricating three-dimensional alkaline graphene oxide (3DGO11) using a facile freeze-drying method for an efficient OH^- conductor. Compared to the 2DGO11, the current approach of 3DGO11 through a freeze-drying route ensures high porosity, enabling ion conduction in multiple directions with shorter pathways. The increased surface area and porosity facilitate high water absorption, ultimately leading to elevated hydroxide ion conductivity. Our study contributes to the advancement of graphene oxide applications in electrochemical energy conversion devices, offering a promising alternative to conventional fabrication methods.

2. Experimental

All reagents and chemicals utilized were of analytical grade and used without further purification.

2.1. Fabrication of graphene oxide

Graphite oxide was obtained by using a modified Hummers' method.[16] Typically, a round bottom flask containing graphite (1 g), sodium nitrate (1 g), and sulfuric acid (97%, 48 mL) was cooled and stirred for about half an hour. Then, finely ground potassium permanganate (3 g) was slowly added to the above mixture under stirring and continued for an additional 30 minutes while keeping the reaction temperature below 20 °C. Subsequently, the temperature of the medium was increased to 35 °C and maintained for about 30 minutes. Then water (180 mL) was gradually added to the reaction medium, the temperature was slowly increased to 95 °C, and the mixture was stirred for 30 minutes. Finally, water (400 mL), hydrogen peroxide (30%, 12 mL), and the product were purified using 5% HCl and water. The product was dried at 80 °C overnight as graphite oxide. GO was obtained by dispersing the appropriate amount of graphite oxide in water through sonication for 1 h and centrifuged at 3800 rpm for 30 min. Alkaline graphene

oxide was prepared by adjusting the pH of the graphene oxide dispersion to pH = 11 using a dilute ammonia solution. For 2D alkaline GO (2DGO11), the as-prepared alkaline GO dispersion was vacuum filtered under reduced pressure using a membrane filter with a pore size of 0.45 μm followed by drying under ambient conditions. For three-dimensional alkaline GO (3DGO11), the dispersed alkaline GO solution was freeze-dried (FD-1000, EYELA) for 3 days. Finally, a pellet of 3DGO11 was fabricated using a pressure of 10 MPa.

2.2. Materials characterizations

Field emission scanning electron microscopy (FE-SEM, JSM-7600F, JEOL), X-ray photoelectron spectroscopy (Theta Probe, Thermo Fisher Scientific), thermogravimetry (TGA/DTA 6300, Seiko Instruments Incorporation Ltd), FTIR, and powder X-ray diffraction were used to examine the structural and morphological properties of the synthesized materials.

2.3. Evaluation of ionic conductivity

The ionic conductivity was evaluated using the alternating current (AC) impedance method using an impedance analyzer (MTZ-35, BioLogic Instruments). The ionic conductivity was measured by applying a frequency range of 1–10^6 Hz along with through-plane and in-plane directions. During the measurement, humidity and temperature were regulated using an incubator (IW223, Yamato Scientific Co) to examine the effect of these parameters on the ion-conducting behavior of the as-synthesized membrane. In the case of in-plane conductivity, each membrane was set in the middle of two copper electrodes, and for through-plane conductivity, both sides of the film were coated with gold paste, and each of these sides was connected using gold wire (Au, 50 μm Tanaka Kikinzoku Kogyo K. K.). Finally, conductivity (through-plane) was calculated with the help of the following equation:

$$\sigma = d/SR \quad (1)$$

S is the electrode area, R is the resistance determined by the matching cole–cole plots, and d is the film thickness.

To determine the in-plane ionic conductivity, the following equation was used:

$$\sigma = d/TLR \quad (2)$$

In this case, T denotes the film's thickness, d is the distance between the two electrodes, R is the predicted resistivity derived from the cole–cole plots, and L is the length of the membrane perpendicular to d.

2.4. Determination of water uptake and swelling ratio

The membrane was immersed in N_2 saturated deionized water at room temperature for 1 day. The hydrated membrane was taken out of the water and the excess water was removed using tissue paper and the mass was measured (W_{wet}). The membrane was then dried under a vacuum until a constant dry weight (W_{dry}) was obtained. The water uptake was calculated using the following equation:

$$W\,(\%) = \frac{W_{wet} - W_{dry}}{W_{dry}} \times 100\%$$

The swelling ratio was evaluated by a linear expansion ratio, which was calculated by the difference in the dimensions of the membrane under wet and dry conditions using the following equation:

$$\text{Swelling ratio}\,(\%) = \frac{X_{wet} - X_{dry}}{X_{dry}} \times 100\%$$

Here, X_{wet} and X_{dry} are the lengths of the membrane under wet and dry conditions, respectively.

2.5. Determination of ion exchange capacity (IEC)

The ion exchange capacity (IEC) of the as synthesized membrane was evaluated using the back titration method. The vacuum dried membrane was immersed in 0.01 M HCl standard solution for 24 h. The solution was then titrated with a standardized NaOH solution using phenolphthalein as an indicator. The IEC value was calculated using the following equation:

$$\text{Ion exchange capacity} = \frac{V_{0,NaOH} C_{NAOH} - V_{x,NaOH} C_{NaOH}}{m_{dry}}$$

Here, $V_{0,NaOH}$ and $V_{x,NaOH}$ are the volumes of NaOH consumed in the titration without and with membranes, respectively. C_{NaOH} is the molar concentration of NaOH and m_{dry} is the mass of the dried membrane. Three replicates were conducted for the membrane.

2.6. Evaluation of the type of ion conduction

The characterization of ion-conducting species in both three-dimensional graphene oxide (3DGO) and the three-dimensional alkaline graphene oxide (3DGO11) membrane was conducted by assessing the electromotive force (EMF). Measurement was also done for a commercial proton exchange membrane (Nafion 117) and anion exchange membrane (PEEK-Reinforced, 130 μm, Fumasep@ FAA-3-PK-130). These experiments were carried out utilizing water vapor concentration cells under controlled conditions of 30 °C and 80% relative humidity. Throughout the experiment, a stream of humidified and desiccated oxygen gas flowed from two distinct sides of the cell, with the respective membrane positioned between a pair of stainless mesh electrodes for each measurement. Electromotive forces were precisely recorded as open-circuit potentials or electrical voltages, representing the charge separation occurring across the membrane. The open-circuit voltage data were collected using a Keithley 2100 series: a 6.5-digit multimeter manufactured by Tektronix Company, providing accurate and reliable measurements during the evaluation process. This approach allowed for a comprehensive analysis of the ion-conducting behavior of both GO and 3DGO11 membranes, contributing valuable insights to the understanding of their

electrochemical properties under specific environmental conditions.

3. Results and discussion

3.1. Characterizations of the 3DGO hybrid

The surface morphology and chemical properties of the prepared 3DGO11 are illustrated in Fig. 1. A comparative analysis was conducted with as-prepared GO and 2DGO11. The scanning electron microscope (SEM) images of unpressed 2DGO11 and 3DGO11 are presented in Fig. 1a and b, respectively, showcasing the characteristic sheet structure of GO. The layer structure of the corresponding membrane is discernible in the cross-section SEM image of 2DGO11 and 3DGO11 in Fig. 1(c) and (d). Fig. S1 (ESI†) shows the photographs of the 3DGO11 sample and the corresponding membrane. Membrane flexibility was observed from the optical images in Fig. S1(c) (ESI†). Fig. 1(e) displays the powder X-ray diffraction (PXRD) patterns of 2DGO11 and 3DGO11. In particular, 2DGO11 exhibits a peak at a 2θ value of 10.2 degrees with an interlayer distance of 0.87 nm. In contrast, 3DGO11 manifests a peak at 9.92 degrees while maintaining an interlayer distance of 0.89 nm. The interlayer is enhanced due to the three-dimensional formation of GO, which is in line with previous reports. Fig. S2 (ESI†) shows the typical atomic force microscopy (AFM) images of 3DGO11. The AFM images show the sheet like structures with sharp edges and also the formation of single layer nanosheets. Furthermore, the porous nature of 3DGO11 was confirmed by the nitrogen adsorption–desorption measurement (Fig. S4, ESI†). The BET-specific surface area of the prepared 3DGO11 was 19.3 $m^2\ g^{-1}$, which is advantageous for higher water absorption and ionic conductivity. X-ray photoelectron spectroscopy (XPS) analysis in Fig. 1(f) and (g) for GO and 3DGO11, respectively, confirms the conversion of epoxy functional groups of GO due to the change in pH. In the XPS spectra, characteristic peaks appear in the range of 284–286 eV for carbon-based bonds, including C–H, C–C, and C–O bonds. The distinctive peaks associated with oxygenated functional groups encompass hydroxyl (C–OH), epoxy (C–O–C), carbonyl (–C═O), and carboxyl (–COOH) groups, with peak intensities approximately situated at 286.4–286.6 eV, 286.8–287.0 eV, 287.8–288.0 eV, and 289.0–289.3 eV, respectively.[22] Notably, the peak intensity at 286.8–287.0 eV, corresponding to the epoxy group, is significantly higher in GO compared to that of 3DGO11, indicating the presence of a substantial number of epoxy (C–O–C) groups in GO. Conversely, the peak intensity in the hydroxyl group at 286.4–286.6 eV is greater in the case of 3DGO11 compared to that of GO. Additionally, measurement of the FTIR spectra for both GO and 3DGO11 (Fig. S3, ESI†) showed that some of the functional groups in GO were changed during the synthesis of 3DGO11 from GO. In particular, the peaks located at 1729.6, 1632, 1300 and 1052 cm^{-1} correspond to the stretching frequencies of –C═O (carboxyl and carbonyl), –C═C– (aromatic sp^2 carbon), –C–O–C– (epoxy) and –COH (hydroxyl) functional groups, respectively.[24] The broad intense band at around 3350 cm^{-1} indicates the presence of hydroxyl groups or the water molecules adsorbed on the hydrophilic functional sites of GO. For GO(11), the relative intensities of the peaks at 3350 and 1050 cm^{-1}, attributed to the –C–OH groups, increase while the peak intensity at 1300 cm^{-1} attributed to the –C–O–C– functional groups decreases. This evidence confirms that the conversion of epoxy to hydroxyl groups occurred during the conversion of GO to 3DGO11.

3.2. Measurement of the nature of ionic conductivity, water uptake, swelling ratio and value of ion conduction

The investigation into the conducting ion nature within GO and 3DGO involved the utilization of a concentration cell with water

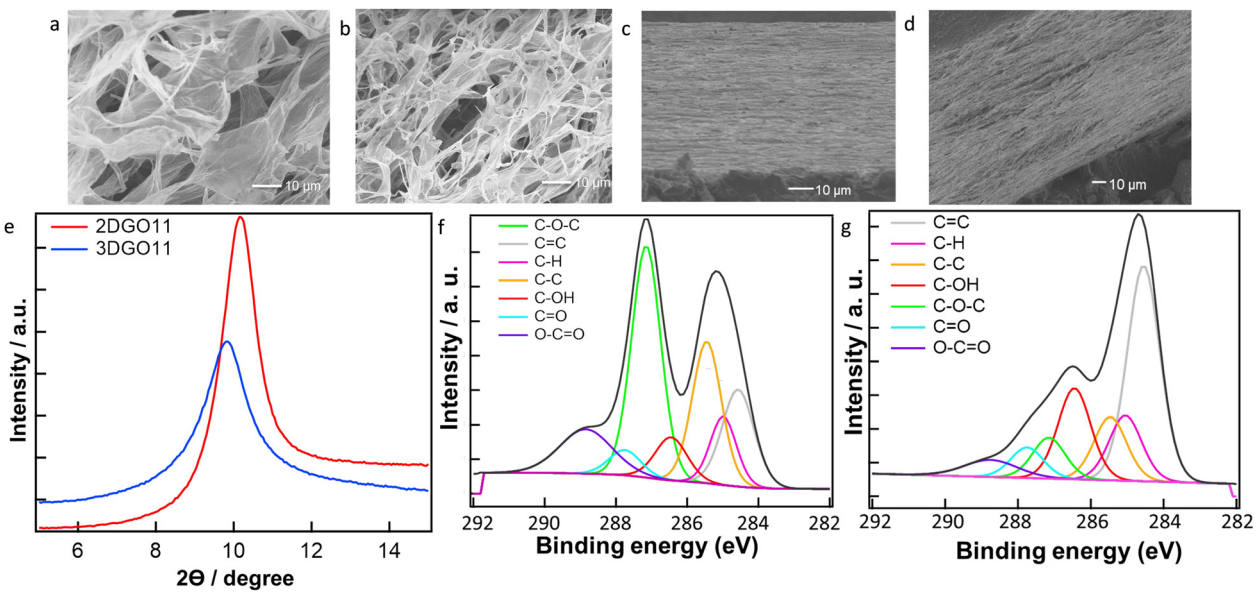

Fig. 1 Surface morphology and chemical properties of the prepared materials. (a) SEM images of un-pressed 2DGO11, and (b) 3DGO11; (c) SEM images for the cross section of pressed 2DGO11, and (d) pressed 3DGO11; (e) PXRD pattern of 2DGO11 and 3DGO11; (f) C 1s XPS spectra of GO and (g) 3DGO11.

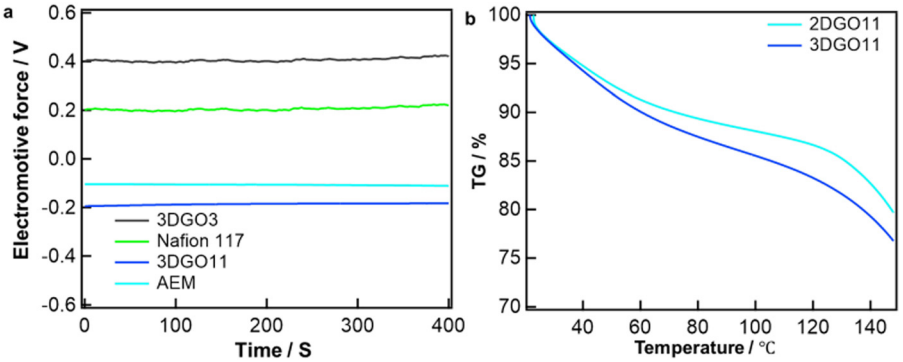

Fig. 2 (a) Identification of the type of ion conduction: measurement of the EMF value using a water vapor concentration cell using Nafion, AEM, 3DGO3 and 3DGO11 as electrolytes; (b) weight loss profiles were discovered using TGA analysis in an N_2 environment for 2DGO11 and 3DGO11.

vapor.[22,25] Fig. 2a shows the variation in electromotive force (EMF) over time using both GO, 3DGO11, Nafion and the anion exchange membrane. The EMF's sign serves as a crucial indicator to comprehend the type of ion conduction taking place in the respective membrane. Typically, a positive EMF signifies cationic conduction, while anionic conductors exhibit a negative EMF.[22] For comparison, incorporating 3DGO11 and AEM into the concentration cell resulted in a negative EMF value, contrasting with the positive EMF observed for GO and Nafion 117. This unmistakably indicates that the nature of ion conduction in 3DGO11 involves hydroxide ions.[25] The observed result also supports our previous work. Furthermore, Fig. 2b presents the outcomes of a thermogravimetric analysis (TGA) conducted in a nitrogen atmosphere. The weight fraction of each sample gradually diminishes during the heating process, reaching up to approximately 100 °C. This reduction likely indicates the release of moisture trapped within the GO interlayer. Specifically, for 3DGO11, there is a weight loss of 15%, in contrast to the 12% weight loss observed for 2DGO11 when the materials are heated up to 100 °C. The amount of adsorbed water is of particular importance as it directly influences ionic (H^+ or OH^-) conductivity, a critical factor in fuel cell operation. Furthermore, it is worth noting that fuel cells typically operate under high humidity conditions, allowing for the recovery of the lost water content during operation, thus maintaining stable performance.

The higher weight loss in 3DGO11 compared to 2DGO11 can be attributed to the increased porosity achieved through the

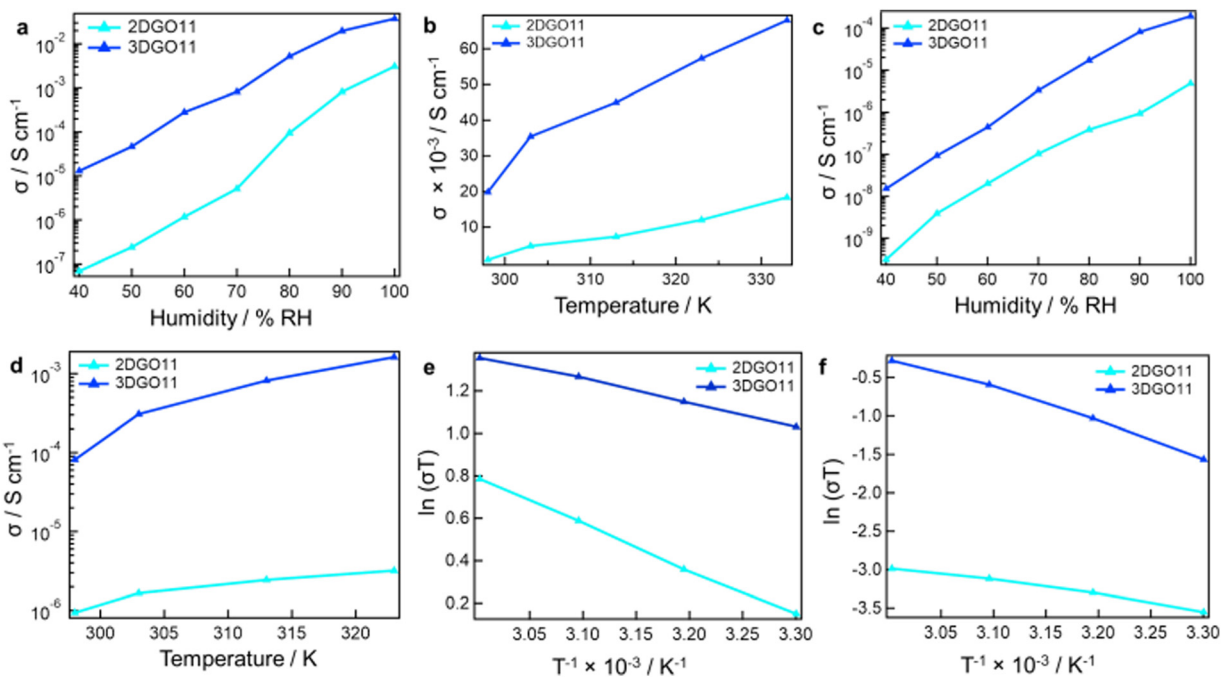

Fig. 3 OH^- conductivities of 2DGO11 and 3DGO11: humidity dependent OH^- conductivity in the (a) in-plane and (c) through-plane direction measured maintaining several humidified conditions at 25 °C; temperature-dependent OH^- conductivity in the (b) in-plane and (d) through-plane direction measured at different temperatures under 90% RH; Arrhenius plots of $\ln(\sigma T)$ *vs.* T^{-1} for (e) in-plane pathways and (f) the through-plane route evaluated at 90% RH.

freeze-drying method.[24] Furthermore, the measurement of water uptake and swelling ratio (Fig. S5, ESI†) shows that 3DGO11 has higher water uptake and degree of swelling than that of 2DGO11. Measurement of the ion exchange capacity reflects the exchangeable functional group in the membrane, which plays a key role in determining the conductivity of the ionomer. The experimental IEC value was 1.75 mequiv g^{-1}.

Ionic conductivity measurements were conducted for both in-plane and through-plane directions using 2DGO11 and 3DGO11, with variations in humidity and temperature. The results are depicted in Fig. 3. It is evident that the ionic conductivity values increase with the rise in relative humidity (RH) at 25 °C (Fig. 3a). For 2DGO11, an ionic conductivity value of 6.89×10^{-8} S cm^{-1} was observed at 40% RH, reaching 3.08×10^{-3} S cm^{-1} at 100% RH. In contrast, 3DGO11 exhibited a σ-value of 1.30×10^{-5} S cm^{-1} at 40% RH compared to 3.75×10^{-2} S cm^{-1} at 100% RH, making the σ-value of 3DGO11 10 times higher than that of 2DGO11. For through-plane ionic conductivity in Fig. 3c, 2DGO11 yielded a value of 3.08×10^{-10} S cm^{-1} at 40% RH, increasing to 4.82×10^{-6} S cm^{-1} at 100% RH. In contrast, 3DGO11 exhibited a conductivity value of 1.52×10^{-8} S cm^{-1} at 40% RH compared to 1.39×10^{-4} S cm^{-1} under the optimum humidified conditions, with the through-plane ionic conductivity of 3DGO11 being 40 times higher than that of 2DGO11. The conductivity values of 2DGO11 and 3DGO11 were evaluated at 90% RH while adjusting the temperature, as illustrated in Fig. 3(b) and (d) for in-plane and though-plane, respectively. The σ-values exhibited the expected incremental trend for each sample, reflecting the influence of temperature on ionic conductivity. Fig. 3(e) and (f) shows the activation energies (E_a) for both the in-plane and through-plane directions. The calculated activation energies for the in-plane direction were 0.19 eV and 0.09 eV for 2DGO11 and 3DGO11, respectively. Conversely, the E_a values in the through-plane directions were 0.18 and 0.10 eV for 2DGO11 and 3DGO11, respectively. These values suggest that the Grotthuss mechanism is responsible for hydroxide ion transfer.

The higher in-plane hydroxide conductivity compared to through-plane conductivity can be attributed to the structural arrangement and morphology of the GO membrane. Within the in-plane direction of GO, there exists a high degree of connectivity between the functional groups, creating pathways for efficient proton transport. In contrast, the stacking of GO layers in the through-plane direction leads to interlayer spacing that hinders the mobility of hydroxide between the layers, resulting in reduced conductivity. Additionally, the in-plane orientation of the GO sheets often offers more favorable morphological features, such as higher surface area and greater accessibility to functional groups, further enhancing ionic conductivity in this direction.

The ionic (H^+/OH^-) conductivity mechanism in 2D layered nanosheet materials, such as graphene oxide (GO)-based membranes, primarily involves the self-dissociation of adsorbed water molecules, leading to the generation of H^+/OH^- ions. Subsequently, these ions undergo rapid propagation *via* the Grotthuss mechanism, which involves the breaking and reformation of hydrogen bonds, facilitated by the presence of hydrophilic functional groups on the GO surface, including hydroxyl, epoxy, and carboxyl groups. The transportation of H^+ ions is well understood, involving continuous interconversion between adjacent hydrated (H_3O^+) complexes and the formation of a hydrogen-bonding network with water molecules. However, the mechanism of OH^- ion conduction under humidified conditions remains under investigation. In alkaline environments, such as those encountered in GO-based membranes, epoxy groups can convert to OH^- ions, maintaining the water between the layers in a basic state. The movement of OH^- ions is thought to be accompanied by the formation of clusters containing multiple water molecules, known as $OH^-(H_2O)_n$ arrangements, wherein a hyper-coordinating water molecule facilitates the ion's mobility.[25] Further research is ongoing to elucidate the precise mechanisms governing OH^- ion conduction in such systems.[22] Nevertheless, the nature of ionic conductivity involved in 3DGO11 was confirmed through water vapor experiments (Fig. 2a).

The 3D structural arrangement in 3DGO11 was achieved through a freeze-drying synthesis route. In this process, the alkaline GO suspension in aqueous media undergoes freezing. As the ice forms, the entire volume expands, causing nearby particles to be further separated, and the relative positions of the particles become fixed, no longer free to approach each other. This leads to the interfacial tension between water molecules and the solid particles being much weaker than that occurring between liquid water molecules and the particles. Consequently, the aggregation of particles is prevented. The outcome is a distinctive, lightweight, three-dimensional pore-rich hierarchical 3DGO11 framework with a high internal surface area and flexibility.[24] This process has numerous attachment sites, establishing an efficient OH^- conduction pathway. Furthermore, 3DGO11 demonstrates a higher interlayer distance compared to 2DGO11. The relatively low OH^- conductivity observed in 2DGO11 is attributed to the restacking behavior of graphene oxide during fabrication, leading to an extended conduction pathway and fewer conduction routes. This difference results in higher water uptake and enhanced hydroxide ion conductivity in the 3DGO11 membrane. The distinct features of 3DGO11, including its porosity, nanopore interconnectivity, and increased interlayer distance, collectively contribute to its superior performance as an efficient OH^- conductor.[21,24]

4. Conclusions

The current study successfully demonstrates the fabrication of a three-dimensional alkaline graphene oxide membrane (3DGO11) through a facile freeze-drying method. The resulting membrane exhibits exceptional in-plane and through-plane OH^- conductivity, marking a substantial advancement in alkaline graphene oxide electrolytes. Notably, the 3DGO11 membrane achieves an outstanding 40-fold increase in ion conductivity in the through-plane direction compared to a 2D

alkaline graphene oxide membrane. In the in-plane direction, the OH^- conductivity of 3DGO11 surpasses that of its 2D counterpart by a factor of 10. These remarkable conductivity improvements underscore the three-dimensional structure's effectiveness in promoting ion transport, providing a substantial advantage over traditional two-dimensional membranes. Our findings contribute to the scientific understanding of graphene oxide-based electrolytes and offer valuable insights for developing future anion exchange membrane fuel cells (AEMFCs). By showcasing the superior performance of 3D GO11, we anticipate that our research will serve as a foundation for the design and optimization of advanced materials, paving the way for the next generation of AEMFCs with enhanced efficiency and reliability. This work opens up exciting possibilities for the practical application of three-dimensional alkaline graphene oxide membranes in electrochemical energy conversion devices, bringing us closer to sustainable and efficient energy solutions.

Conflicts of interest

There are no conflicts to declare.

Acknowledgements

This work was supported by the JSPS KAKENHI Grant number 22K19053.

Notes and references

1 (*a*) M. Vinothkannan, A. R. Kim, G. G. kumar, J.-M. Yoond and D. Jin Yoo, *RSC Adv.*, 2017, **7**, 39034–39048; (*b*) Y. Wang, D. F. R. Diaz, K. S. Chen, Z. Wang and X. C. Adroher, *Mater. Today*, 2020, **32**, 178–203.

2 N. Ralbag, M. Mann-Lahav, E. S. Davydova, U. Ash, R. Galed, M. Handl, R. Hiesgen, E. Magliocca, W. Mustain, J. He, P. Cong, A. M. Beale, G. S. Grader, D. Avnir and D. R. Dekel, *Matter*, 2019, **1**, 959–975.

3 M. Bellini, M. V. Pagliaro, A. Lenarda, P. Fornasiero, M. Marelli, C. Evangelisti, M. Innocenti, Q. Jia, S. Mukerjee, J. Jankovic, L. Wang, J. R. Varcoe, C. B. Krishnamurthy, I. Grinberg, E. Davydova, D. R. Dekel, H. A. Miller and F. Vizza, *ACS Appl. Energy Mater.*, 2019, **2**, 4999–5008.

4 D. R. Dekel, *ECS Trans.*, 2013, **50**, 2051–2052.

5 S. J. Peighambardoust, S. Rowshanzamir and M. Amjadi, *Int. J. Hydrogen Energy*, 2010, **35**, 9349–9384.

6 M. Karim, K. Hatakeyama, M. Koinuma and S. Hayami, *J. Mater. Chem. A*, 2017, **5**, 7243–7256.

7 H.-S. Dang and P. Jannasch, *J. Mater. Chem. A*, 2016, **4**, 11924–11938.

8 J. P. González, D. K. Whelligan, L. Wang, R. B. Soualhi, Y. Wang, Y. Peng, H. Peng, D. C. Apperley, H. N. Sarode, T. P. Pandey, A. G. Divekar, S. Seifert, A. M. Herring, L. Zhuangb and J. R. Varcoea, *Energy Environ. Sci.*, 2016, **9**, 3724–3735.

9 (*a*) C. Chen, J. Pan, J. Han, Y. Wang, L. Zhu, M. A. Hickner and L. Zhuang, *J. Mater. Chem. A*, 2016, **4**, 4071–4081; (*b*) K. H. Lee, J. Y. Chu, A. R. Khan and D. J. Yoo, *ACS Sustainable Chem. Eng.*, 2021, **9**(26), 8824–8834; (*c*) I. Arunkumar, A. R. Khan, S. H. Lee and D. J. Yoo, *Int. J. Hydrogen Energy*, 2024, **52**, 139–153; (*d*) R. Gokulapriyan, I. Arunkumar, H.-K. Lee and D. J. Yoo, *ACS Appl. Energy Mater.*, 2023, **6**(24), 11549–12559.

10 J. R. Varcoe, P. Atanassov, D. R. Dekel, A. M. Herring, M. A. Hickner, P. A. Kohl, A. R. Kucernak, W. E. Mustain, K. Nijmeijer, K. Scott, T. Xuk and L. Zhuang, *Energy Environ. Sci.*, 2014, **7**, 3135–3191.

11 G. Merle, M. Wessling and K. Nijmeijer, *J. Membr. Sci.*, 2011, **377**(1), 1–35.

12 A. a Balandin, *Nat. Mater.*, 2011, **10**(8), 569–581.

13 N. V. Medhekar, A. Ramasubramaniam, R. S. Ruoff and V. B. Shenoy, *ACS Nano*, 2010, **4**, 2300–2306.

14 K. Erickson, R. Erni, Z. Lee, N. Alem, W. Gannett and A. Zettl, *Adv. Mater.*, 2010, **22**, 4467–4472.

15 S. Islam Md, Y. Shudo and S. Hayami, *Bull. Chem. Soc. Jpn.*, 2022, **95**, 1–25.

16 M. R. Karim, K. Hatakeyama, T. Matsui, H. Takehira, T. Taniguchi, M. Koinuma, Y. Matsumoto, T. Akutagawa, T. Nakamura, S. Noro, T. Yamada, H. Kitagawa and S. Hayami, *J. Am. Chem. Soc.*, 2013, **135**, 8097.

17 M. A. Rahman, N. N. Rabin, M. S. Islam, M. Fukuda, J. Yagyu, Z. Feng, Y. Sekine, L. F. Lindoy, J. Ohyama and S. Hayami, *Chem. – Asian J.*, 2022, e202200376.

18 K. Hatakeyama, M. R. Karim, C. Ogata, H. Tateishi, A. Funatsu, T. Taniguchi, M. Koinuma, S. Hayami and Y. Matsumoto, *Angew. Chem., Int. Ed.*, 2014, **53**, 6997–7000.

19 M. A. Rahman, M. S. Islam, M. Fukuda, J. Yagyu, Z. Feng, Y. Sekine, L. F. Lindoy, J. Ohyama and S. Hayami, *ChemPlusChem*, 2022, **87**(4), e202200003.

20 M. R. Karim, M. S. Islam, K. Hatakeyama, M. Nakamura, R. Ohtani, M. Koinuma and S. Hayami, *J. Phys. Chem. C*, 2016, **120**, 21976–21982.

21 M. A. Rahman, J. Yagyu, M. S. Islam, M. Fukudaa, S. Wakamatsu, R. Tagawa, Z. Feng, Y. Sekine, J. Ohyama and S. Hayami, *ACS Appl. Nano Mater.*, 2023, **6**(3), 1707–1713.

22 M. Fukuda, M. S. Islam, Y. Shudo, J. Yagyu, L. F. Lindoy and S. Hayami, *Chem. Commun.*, 2020, **56**, 4364–4367.

23 T. Taniguchi, S. Kurihara, H. Tateishi, K. Hatakeyama, M. Koinuma, H. Yokoi, M. Hara, H. Ishikawa and Y. Matsumoto, *Carbon*, 2015, **84**, 560–566.

24 J. Yagyu, M. S. Islam, Y. Shudo, M. Fukuda, H. Ushijima, H. J. Ohyama, S. Ida, L. F. Lindoy and S. Hayami, *ACS Appl. Energy Mater.*, 2021, **4**, 6296–6301; K. Tadanaga, Y. Furukawa, A. Hayashi and M. Tatsumisago, *Adv. Mater.*, 2010, **22**, 4401–4404; M. Acik, C. Mattevi, C. Gong, G. Lee, K. Cho, M. Chhowalla and Y. Chabal, *ACS Nano*, 2010, **4**, 5861–5868.

25 (*a*) P. Sun, R. Ma and T. Sasaki, *Chem. Sci.*, 2018, **9**, 33–43; (*b*) N. Agmon, H. Bakker, R. Campen, R. Henchman, P. Pohl, S. Roke, M. Thamer and A. Hassanali, *Chem. Rev.*, 2016, **116**, 7642–7672.